J Math Imaging Vis (2011) 41:194–209
DOI 10.1007/s10851-011-0269-z

New Variational Formulations for Level Set Evolution Without Reinitialization with Applications to Image Segmentation

Chunxiao Liu · Fangfang Dong · Shengfeng Zhu · Dexing Kong · Kefeng Liu

Published online: 3 March 2011

Abstract Interface evolution problems are often solved elegantly by the level set method, which generally requires the time-consuming reinitialization process. In order to avoid reinitialization, we reformulate the variational model as a constrained optimization problem. Then we present an augmented Lagrangian method and a projection Lagrangian method to solve the constrained model and propose two gradient-type algorithms. For the augmented Lagrangian method, we employ the Uzawa scheme to update the Lagrange multiplier. For the projection Lagrangian method, we use the variable splitting technique and get an explicit expression for the Lagrange multiplier. We apply the two approaches to the Chan-Vese model and obtain two efficient alternating iterative algorithms based on the semi-implicit additive operator splitting scheme. Numerical results on various synthetic and real images are provided to compare our methods with two others, which demonstrate effectiveness and efficiency of our algorithms.

Keywords Level set method · Reinitialization · Augmented Lagrangian method · Projection Lagrangian method · Chan-Vese model · Additive operator splitting

C. Liu (✉) · K. Liu
Center of Mathematical Sciences, Zhejiang University, Hangzhou 310027, P.R. China
e-mail: xxliu198431@126.com

F. Dong
School of Statistics and Mathematics, Zhejiang Gongshang University, Hangzhou 310018, P.R. China

S. Zhu · D. Kong
Department of Mathematics, Zhejiang University, Hangzhou 310027, P.R. China

1 Introduction

Interface evolution occurs in a wide variety of settings such as image precessing, computer vision, shape optimization and geometric inverse problems. Most traditional explicit front tracking algorithms place marker points along the interface and advance the position of these points through an evolution equation. However, expensive reparametrization is necessary during the evolution and the topology of the subregions separated by the interface cannot change automatically. The level set method (LSM) originally proposed by Osher and Sethian [1] for interface tracking can overcome these two main drawbacks. Effective and efficient numerical schemes can be implemented on fixed grids. Moreover, it can handle topological changes such as merging, splitting and forming sharp corners. The essential idea of the LSM is to implicitly embed the propagating interface as the zero level set of a higher dimensional level set function (LSF). With this representation, the motion of the interface is described by a time dependent Hamilton-Jacobi type evolution equation of the LSF. The LSM has been applied in many fields including optimal shape design [2, 3], computational fluid dynamics [4], inverse problems [5, 6], image processing [7, 8], etc. For more details on the LSM and its applications, we refer to [9–11].

During the level set evolution, regularity is often needed to impose on the LSF to prevent it to be too steep or too flat near the interface. This is normally done by requiring it to be a signed distance function. The process is commonly known as reinitialization, which is used extensively as a numerical strategy for maintaining interface evolution stable (cf. [9, 10]). However, there are some drawbacks for reinitialization (cf. [9, 12–14]). For the Chan-Vese (CV) model [15] in the image segmentation task, whether or not the reinitialization is processed affects the topology of the resulting image for some special images [13]. It still remains

to be a problem when and how to implement reinitialization [12, 14].

There are several effective ways to implement reinitialization. Sethian [16, 17] developed the fast marching method to efficiently calculate the signed distance function by solving the Eikonal equation on both sides of the interface. Another efficient algorithm for solving this equation is the fast sweeping method (cf. [18]). Sussman et al. [4] proposed a time dependent PDE based iterative algorithm to satisfy the Eikonal constraint equation. For some cases requiring velocity extension, the fast marching method can be used to construct a velocity field, which simultaneously avoids reinitialization (cf. [19]). In [20], a PDE based fast algorithm implemented on a narrow band tube of the interface was suggested to extend the velocity and implement reinitialization. As interesting variants of the traditional LSM, level set algorithms of piecewise constant type [13, 21–23] also eliminate the need of reinitialization. These methods require to handle additional piecewise constant constraints.

To avoid reinitialization, Li et al. [14] proposed a variational formulation and applied it to the geodesic active contour model for image segmentation. They added a quadratic penalty term into the original energy functional in order to force the LSF to be a signed distance function during evolution. Therefore, the algorithm they provided is essentially based on a classical quadratic penalty method for constrained optimization (cf. [24]). By forcing the weight of the constraint term to infinity, one can penalize the constraint violations with increasing severity. That is, the larger weight one uses, the closer the LSF is to a signed distance function. However, the Courant-Friedrichs-Lewy (CFL) stability condition for explicit discretization of the gradient descent flow does not allow the weight value to be large, or else the time step has to be small and the iteration is rather slow. Therefore, there is a contradiction between the accuracy of the constraint and the choice of large time steps. In numerical experiments of [14], large time steps were employed at the expense of small weight values.

In this paper, we propose two more accurate constrained optimization approaches, an augmented Lagrangian method and a projection Lagrangian method, to get rid of reinitialization in the level set evolution. For the projection Lagrangian method, we construct a new scheme to update the Lagrange multiplier using the variable splitting technique by introducing an auxiliary variable [25–27]. Then we apply our methods to the well-known CV model (cf. [15, 28, 29]), which is an especially useful model when the image to be segmented can be approximated by piecewise constant functions. The additive operator splitting (AOS) scheme is employed in solving the obtained nonlinear diffusion equation. Numerical results show that our methods are effective and less sensitive to noise. Comparing with the LSM with reinitialization and the penalty method of [14] applying to the CV model, our algorithms work much faster.

The rest of this paper is organized as follows. In Sect. 2, some existing results related to the LSM and reinitialization process are briefly stated. In Sect. 3, our new methods are proposed in detail. Then we apply our methods to the CV model and devise two robust algorithms in Sect. 4. Numerical examples are presented in Sect. 5. Finally, we give a brief summary and outline the future work in Sect. 6.

2 Related Works

2.1 Traditional LSM

We first recall the basic level set formulations. Let $\Omega \subset \mathbb{R}^d$ $(d = 2, 3)$ be an open bounded domain and $\{\Gamma(t) \mid t \geq 0\}$ be a series of moving closed interfaces in Ω with velocity $v = x'(t)$. For some t, $\Omega_1(t)$ and $\Omega_2(t)$ are two subregions separated by $\Gamma(t)$. Define a Lipschitz continuous LSF $\phi(x,t)$ satisfying

$$\begin{cases} \phi(x,t) < 0, & x \in \Omega_1(t), \\ \phi(x,t) = 0, & x \in \Gamma(t), \\ \phi(x,t) > 0, & x \in \Omega_2(t). \end{cases} \tag{1}$$

The evolution equation of $\Gamma(t)$ can be transformed into that of $\phi(x,t)$. Specifically, differentiating the equation $\phi(x(t),t) = 0$ with respect to t reads:

$$\phi_t + v \cdot \nabla\phi = 0. \tag{2}$$

By restricting the front to propagating along its normal direction with speed v_n, (2) turns to the so-called level set equation

$$\phi_t + v_n|\nabla\phi| = 0. \tag{3}$$

The velocity v_n can be a function of the normal direction, mean curvature, etc.

In order to keep stability in numerical implementation, often regularity is imposed on the LSF to ensure $0 < c \leq |\nabla\phi| \leq C$, for some constants c and C. Actually, it is very desirable to require it to be a signed distance function, i.e.,

$$\phi(x,t) = \begin{cases} -d(\Gamma(t),x), & x \in \Omega_1(t), \\ 0, & x \in \Gamma(t), \\ d(\Gamma(t),x), & x \in \Omega_2(t), \end{cases} \tag{4}$$

where $d(\Gamma(t),x)$ denotes the Euclidean distance from x to $\Gamma(t)$. An equivalent constraint to (4) is the Eikonal equation

$$|\nabla\phi(x,t)| = 1. \tag{5}$$

In order to satisfy (5), the authors of [4] used an iterative reinitialization scheme to solve the following equation to steady state:

$$\begin{cases} \phi_t + \operatorname{sign}(\phi_0)(|\nabla\phi| - 1) = 0 & \text{in } \Omega \times \mathbb{R}^+, \\ \phi(x,0) = \phi_0 & \text{in } \Omega, \end{cases} \tag{6}$$

where ϕ_0 is the function to be reinitialized and $\text{sign}(\phi_0)$ denotes the sign function of ϕ_0. But this expensive reinitialization approach may cause the interface to move appreciably after many iterations and it cannot reinitialize the LSF which is far away from a signed distance function. These issues can be resolved well by arbitrary interface preserving schemes [30] and an efficient narrow band based algorithm [20]. In the filed of image segmentation, for some images without clear edges, the segmentation results are largely dependent on the manner of reinitialization [12, 14].

2.2 Variational Level Set Method (VLSM)

The VLSM proposed in [31] offers us a way to embed the LSF directly into the energy functional.

Assume that the minimization problem with respect to interfaces is in the following general form:

$$\min_{\Gamma} \mathcal{F}(\Gamma). \tag{7}$$

Then the VLSM embeds the LSF into the energy functional $\mathcal{F}(\Gamma)$ by utilizing the following facts about the Heaviside function and Dirac function:

$$\begin{aligned} &\int_{\Omega_1} f\,dx = \int_{\Omega} f(1 - H(\phi))dx, \\ &\int_{\Omega_2} f\,dx = \int_{\Omega} f H(\phi)dx, \\ &|\Gamma| := \int_{\Gamma} ds = \int_{\Omega} \delta(\phi)|\nabla\phi|dx, \end{aligned} \tag{8}$$

where f is some given function defined on Ω. The Heaviside function $H(x)$ is defined as

$$H(x) = \begin{cases} 1, & x \geq 0, \\ 0, & x < 0. \end{cases} \tag{9}$$

The Dirac function $\delta(x)$ is actually the derivative of the Heaviside function in the distributional sense, i.e.,

$$\delta(x) = \begin{cases} \infty, & x = 0, \\ 0, & x \neq 0. \end{cases} \tag{10}$$

By the VLSM, the minimization problem (7) can be reformulated as

$$\min_{\phi} \mathcal{F}(\phi). \tag{11}$$

The Euler-Lagrange equation of (11) with respect to ϕ is much easier to be derived than that of (7) with respect to Γ. We can use the gradient descent method or other efficient schemes to get an optimal solution of (11). Moreover, we can incorporate any additional information or constraints on the LSF into the variational energy functional.

In numerical implementation, we use the regularized version with parameter $\varepsilon > 0$ to approximate the original non-differentiable function $H(x)$ and $\delta(x)$ respectively as

$$H_\varepsilon(x) = \frac{1}{2} + \frac{1}{\pi}\arctan\frac{x}{\varepsilon} \tag{12}$$

and

$$\delta_\varepsilon(x) = \frac{1}{\pi}\frac{\varepsilon}{x^2 + \varepsilon^2}. \tag{13}$$

As pointed out in [15], this kind of smooth approximations have the tendency to lead a global minimizer of the algorithm.

2.3 Variational Level Set Method Without Reinitialization (VLSMWR)

Using the VLSM and considering the constraint (5), we can formulate the general interface evolution problem as the following constrained minimization problem

$$\min_{\phi} \mathcal{F}(\phi) \quad \text{subject to} \quad |\nabla\phi| = 1. \tag{14}$$

In order to avoid reinitialization in the geodesic active contour model, the authors of [14] added a penalization term into the minimization functional after applying the VLSM and obtained the following unconstrained minimization problem

$$\min_{\phi}\left\{L(\phi) = \mathcal{F}(\phi) + \frac{\mu}{2}\int_{\Omega}(|\nabla\phi| - 1)^2 dx\right\}. \tag{15}$$

The first-order necessary condition leads to

$$\frac{\partial L}{\partial \phi} = \mathcal{F}'(\phi) - \mu\left[\Delta\phi - \nabla\cdot\left(\frac{\nabla\phi}{|\nabla\phi|}\right)\right] = 0. \tag{16}$$

They used the explicit Euler scheme

$$\phi^{k+1} = \phi^k - \Delta t\frac{\partial L}{\partial \phi}(\phi^k) \tag{17}$$

to solve the PDE

$$\begin{cases} \frac{\partial\phi}{\partial t} = -\frac{\partial L}{\partial \phi} & \text{in } \Omega \times \mathbb{R}^+, \\ \phi(x,0) = \phi_0(x) & \text{in } \Omega. \end{cases} \tag{18}$$

It was pointed out in [14] that the time step $\Delta t > 0$ and the penalization parameter $\mu > 0$ must satisfy $\mu\Delta t < 0.25$ for stability. If one choose a relatively large μ, Δt must be rather small in order to satisfy the CFL condition, which means that more iterations are needed to solve (18) to the steady state. On the other hand, we can easily see that this method is essentially a kind of quadratic penalty method for constrained optimization [24]. If μ is too small, we cannot penalize the constraint violation effectively. In order to improve the accuracy and stability, we introduce the following two methods.

3 Two Constrained Optimization Methods

We know from [24] that the quadratic penalty function is not an *exact* penalty function. The constraint will be fulfilled only when the penalty parameter is sufficiently large. However, too large penalty parameters may result in instability. In the following, we use two *exact* methods: the augmented Lagrangian method and the projection Lagrangian method, to force the LSF to be close to a signed distance function so that we can avoid the complicated and expensive reinitialization process. Based on the piecewise constant and binary level set frames, the two methods have been applied to image segmentation [13, 21] and shape optimization [22, 23].

3.1 Augmented Lagrangian Method

Firstly, we use the augmented Lagrangian method to solve (14). The augmented Lagrangian method reduces the possibility of ill-conditioning by introducing explicit Lagrange multiplier estimates at each step into the minimization function. There is a simple but efficient updating scheme, i.e., the Uzawa algorithm. Moreover, the convergence of this algorithm can be guaranteed without increasing μ to a very large value as the penalty method.

Define $K(\phi) = |\nabla\phi| - 1$, then the augmented Lagrangian functional of (14) is

$$L_\mu(\phi, \lambda) = \mathcal{F}(\phi) + \int_\Omega \lambda K(\phi) dx + \frac{\mu}{2}\int_\Omega K^2(\phi) dx, \quad (19)$$

where $\lambda \in L^2(\Omega)$ is the Lagrange multiplier. The penalization parameter $\mu > 0$ should be chosen properly.

A saddle point of L_μ requires that

$$\frac{\partial L_\mu}{\partial \phi} = 0 \quad \text{and} \quad \frac{\partial L_\mu}{\partial \lambda} = 0. \quad (20)$$

In fact, we minimize L_μ with respect to ϕ and maximize L_μ with respect to λ. From the definition of L_μ in (19), we have

$$\frac{\partial L_\mu}{\partial \phi} = \mathcal{F}'(\phi) - \nabla\cdot\left(\lambda\frac{\nabla\phi}{|\nabla\phi|}\right) - \mu\left[\Delta\phi - \nabla\cdot\left(\frac{\nabla\phi}{|\nabla\phi|}\right)\right], \quad (21)$$

$$\frac{\partial L_\mu}{\partial \lambda} = K(\phi). \quad (22)$$

We update ϕ, λ alternatively to find the saddle point starting from the initial guesses ϕ^0 and λ^0.

The updating of ϕ is done by introducing an artificial time variable t and moving in the steepest descent direction by

$$\frac{\partial \phi}{\partial t} = -\frac{\partial L_\mu}{\partial \phi}, \quad (23)$$

Algorithm 1 Uzawa Algorithm for VLSMWR

Choose μ properly, fixed. Initialization: ϕ^0, λ^0, $k = 0$.

Step 1. Update ϕ using the explicit Euler scheme (24) or other semi-implicit schemes, to approximately solve

$$L_\mu(\phi^{k+1}, \lambda^k) = \min_\phi L_\mu(\phi, \lambda^k).$$

Step 2. Update λ by (25).

Step 3. Iterate again if necessary; $k = k + 1$.

where $\partial L_\mu/\partial\phi$ is given by (21). When $t \to \infty$, (23) reaches the steady state $\partial\phi/\partial t = 0$, which implies that $\partial L_\mu/\partial\phi = 0$. In numerical implementation, we can solve equation (23) by the explicit scheme

$$\begin{cases} \phi^{[k,n+1]} = \phi^{[k,n]} - \Delta t^{[k,n]}\frac{\partial L_\mu}{\partial\phi}(\phi^{[k,n]}, \lambda^k), \\ \phi^{[k,0]} = \phi^k, \end{cases} \quad (24)$$

where $n = 0, 1, \ldots, N-1$ in the superscript $[k, n]$ denotes the nth inner iteration corresponding to the kth outer iteration and $\Delta t^{[k,n]} > 0$ is the time step, which should be small enough to ensure the stability of the numerical scheme. A line search method can be applied to find the optimal $\Delta t^{[k,n]}$ at each iteration. Alternatively, considering the time consuming of the line search strategy, we can choose a small fixed Δt by trial and error. We can also employ the semi-implicit schemes to improve the stability and eliminate the time step restriction. After performing N inner iterations, we set $\phi^{k+1} = \phi^{[k,N]}$ to approximately solve (23).

Then we employ the Uzawa algorithm to update the Lagrange multiplier λ by

$$\lambda^{k+1} = \lambda^k + \mu K(\phi^{k+1}). \quad (25)$$

When the iteration of λ converges, we get $K(\phi) = 0$.

In conclusion, we incorporate all the above schemes into the following inner-outer iterative Algorithm 1.

3.2 Projection Lagrangian Method

We can also solve the problem (14) by the Lagrange multiplier approach. Let the penalization parameter in (19) be zero. Then we get the following Lagrangian functional

$$L(\phi, \lambda) = \mathcal{F}(\phi) + \int_\Omega \lambda K(\phi) dx. \quad (26)$$

A saddle point of L requires that

$$\frac{\partial L}{\partial \phi} = \mathcal{F}'(\phi) - \nabla\cdot\left(\lambda\frac{\nabla\phi}{|\nabla\phi|}\right) = 0, \quad (27)$$

$$\frac{\partial L}{\partial \lambda} = K(\phi) = 0. \quad (28)$$

The constraint function in our problem contains the first order derivative of ϕ. With the divergence operation upon λ in (27), we cannot use any similar projection approach in [13] to get an explicit formula of λ by (28). Therefore, we use the variable splitting method by creating a new vector variable, say $\mathbf{p}$, to serve as the argument of the functional K, under the constraint $\mathbf{p} = \nabla\phi$. This leads to following constrained problem

$$\max_{\lambda} \min_{\phi,\mathbf{p}=\nabla\phi} \left\{ \mathcal{F}(\phi) + \int_{\Omega} \lambda(|\mathbf{p}| - 1)dx \right\}. \tag{29}$$

Relaxing the equality constraint $\mathbf{p} = \nabla\phi$ and penalize its violation by the quadratic function, we obtain an approximation of (29)

$$\max_{\lambda} \min_{\phi,\mathbf{p}} \left\{ \mathcal{L}(\phi, \mathbf{p}, \lambda) = \mathcal{F}(\phi) + \int_{\Omega} \lambda(|\mathbf{p}| - 1)dx + \frac{\gamma}{2} \int_{\Omega} |\mathbf{p} - \nabla\phi|^2 dx \right\}, \tag{30}$$

where $\gamma > 0$ is the penalty parameter.

The system of optimality conditions of (30) is

$$\frac{\partial \mathcal{L}}{\partial \phi} = \mathcal{F}'(\phi) - \gamma(\Delta\phi - \nabla \cdot \mathbf{p}) = 0, \tag{31}$$

$$\frac{\partial \mathcal{L}}{\partial \mathbf{p}} = \lambda \frac{\mathbf{p}}{|\mathbf{p}|} + \gamma(\mathbf{p} - \nabla\phi) = 0, \tag{32}$$

$$\frac{\partial \mathcal{L}}{\partial \lambda} = |\mathbf{p}| - 1 = 0. \tag{33}$$

The above three equations must be satisfied at a saddle point of the max-min problem (30).

We can directly optimize the functional in (30). Another way is to solve the corresponding nonlinear system of optimality conditions (31)–(33).

The alternating iterative method of multipliers consists in minimizing $L(\phi, \mathbf{p}, \lambda)$ with respect to ϕ and $\mathbf{p}$, keeping λ fixed, then updating λ for fixed ϕ and $\mathbf{p}$.

Firstly, for fixed λ^k,

$$(\phi^{k+1}, \mathbf{p}^{k+1}) \in \arg\min_{\phi,\mathbf{p}} \left\{ \mathcal{F}(\phi) + \int_{\Omega} \lambda^k(|\mathbf{p}| - 1)dx + \frac{\gamma}{2} \int_{\Omega} |\mathbf{p} - \nabla\phi|^2 dx \right\}. \tag{34}$$

To solve the problem (34), we separate it into the following two sub-problems and update ϕ and $\mathbf{p}$ alternatively.

$$\phi^{k+1} \in \arg\min_{\phi} \left\{ \mathcal{F}(\phi) + \frac{\gamma}{2} \int_{\Omega} |\mathbf{p}^k - \nabla\phi|^2 dx \right\}, \tag{35}$$

$$\mathbf{p}^{k+1} \in \arg\min_{\mathbf{p}} \left\{ \int_{\Omega} \lambda^k |\mathbf{p}| dx + \frac{\gamma}{2} \int_{\Omega} |\mathbf{p} - \nabla\phi^{k+1}|^2 dx \right\}. \tag{36}$$

For updating ϕ, the optimality condition of subproblem (35) is actually (31). Then by the gradient descent method, we find a steady-state solution to the PDE

$$\frac{\partial \phi}{\partial t} = -\frac{\partial \mathcal{L}}{\partial \phi}, \tag{37}$$

where $\partial\mathcal{L}/\partial\phi$ is given by (31). The explicit scheme for solving (37) reads:

$$\phi^{[k,n+1]} = \phi^{[k,n]} - \Delta t^{[k,n]} \frac{\partial \mathcal{L}}{\partial \phi}(\phi^{[k,n]}, \mathbf{p}^k, \lambda^k). \tag{38}$$

Then ϕ^{k+1} is determined similarly as in Algorithm 1.

The minimization with respect to $\mathbf{p}$ in subproblem (36) can be done by obtaining the following closed form:

$$\mathbf{p}^{k+1} = \begin{cases} \nabla\phi^{k+1} - \frac{\lambda \nabla\phi^{k+1}}{\gamma |\nabla\phi^{k+1}|}, & \text{if } |\nabla\phi^{k+1}| > \frac{\lambda}{\gamma}, \\ 0, & \text{else.} \end{cases} \tag{39}$$

The formulation (39) is the weighted shrinkage operator that can be computed in a similar way as the shrinkage operator [25, 32]. This weighted shrinkage is extremely fast and requires only a few operations per element of $\mathbf{p}^{k+1}$.

Finally, we derive the formula of λ by a projection method. Multiplying $\mathbf{p}$ on both sides of (32) and using (33), we obtain the explicit expression of λ as:

$$\lambda = \gamma(\mathbf{p} \cdot \nabla\phi - 1). \tag{40}$$

Then with the updated values of ϕ and $\mathbf{p}$, we have the updating scheme of λ:

$$\lambda^{k+1} = \gamma(\mathbf{p}^{k+1} \cdot \nabla\phi^{k+1} - 1). \tag{41}$$

Now we present the inner-outer iterative projection Lagrangian Algorithm 2.

Algorithm 2 Projection Lagrangian Algorithm for VLSMWR

Choose γ properly, fixed. Initialization: $\phi^0, \mathbf{p}^0, \lambda^0, k = 0$.

Step 1. Update ϕ by the explicit scheme (38) or semi-implicit schemes, to approximately solve

$$\mathcal{L}(\phi^{k+1}, \mathbf{p}^k, \lambda^k) = \min_{\phi} \mathcal{L}(\phi, \mathbf{p}^k, \lambda^k).$$

Step 2. Update $\mathbf{p}$ by (39), to solve

$$\mathcal{L}(\phi^{k+1}, \mathbf{p}^{k+1}, \lambda^k) = \min_{\mathbf{p}} \mathcal{L}(\phi^{k+1}, \mathbf{p}, \lambda^k).$$

Step 3. Update λ by (41).

Step 4. Iterate again if necessary; $k = k + 1$.

Remark 1 A useful stopping criterion should be devised according to the practical problem to be solved. Therefore, we have not and cannot present a unified stopping criterion for either of the above two algorithms based on the general frame of VLSMWR.

4 Applications to the Chan-Vese Model

As a piecewise constant case of the Mumford-Shah model [33], the CV model [15] is one of the classical active contour models in image segmentation. It is usually solved by the VLSM. Therefore, the penalty approach based VLSMWR in [14] can be naturally applied to CV model. In this section, we will apply our two proposed variational methods to the CV model to get rid of reinitialization.

Let $I:\Omega\to\mathbb{R}$ be an image to be segmented. The CV model aims to find an interface which is optimal in that it minimizes the following functional

$$\mathcal{F}(\Gamma,c_1,c_2)=\alpha\int_{\Gamma}ds+\beta_1\int_{\Gamma^{out}}(I-c_1)^2dx+\beta_2\int_{\Gamma^{in}}(I-c_2)^2dx, \tag{42}$$

where Γ^{out} and Γ^{in} are respectively the subregions outside and inside Γ. The constants c_1 and c_2 are the mean intensities of each region separated by Γ. Here, $\alpha>0$ is the weight of the regularization term and $\beta_1,\beta_2>0$ are the weights of the fidelity terms.

Using the variational level set frame, (42) can be transformed to

$$\mathcal{F}(\phi,c_1,c_2)=\alpha\int_{\Omega}\delta_\varepsilon(\phi)|\nabla\phi|dx+\beta_1\int_{\Omega}(I-c_1)^2(1-H_\varepsilon(\phi))dx+\beta_2\int_{\Omega}(I-c_2)^2H_\varepsilon(\phi)dx. \tag{43}$$

We can update c_1, c_2 and ϕ alternately.

Minimizing $\mathcal{F}$ with respect to c_1 and c_2 for some fixed ϕ^k, we obtain

$$c_1^k=\frac{\int_\Omega I\,(1-H_\varepsilon(\phi^k))dx}{\int_\Omega(1-H_\varepsilon(\phi^k))dx}, \tag{44}$$

$$c_2^k=\frac{\int_\Omega I\,H_\varepsilon(\phi^k)dx}{\int_\Omega H_\varepsilon(\phi^k)dx}. \tag{45}$$

Then we can apply our proposed methods in Sect. 3 to the CV model. For the gradient descent flow (23) in the augmented Lagrangian method, we have

$$\frac{\partial\phi}{\partial t}=\mu\Delta\phi+\nabla\cdot\left[(\lambda-\mu)\frac{\nabla\phi}{|\nabla\phi|}\right]+\alpha\delta_\varepsilon(\phi)\nabla\cdot\left(\frac{\nabla\phi}{|\nabla\phi|}\right)+\delta_\varepsilon(\phi)\big[\beta_1(I-c_1)^2-\beta_2(I-c_2)^2\big]. \tag{46}$$

In the projection Lagrangian method, the gradient flow (37) turns to

$$\frac{\partial\phi}{\partial t}=\gamma\Delta\phi+\alpha\delta_\varepsilon(\phi)\nabla\cdot\left(\frac{\nabla\phi}{|\nabla\phi|}\right)+\delta_\varepsilon(\phi)\big[\beta_1(I-c_1)^2-\beta_2(I-c_2)^2\big]. \tag{47}$$

Noting the time step restrictions of the linear and nonlinear diffusion terms in (46) and (47) if explicit schemes are employed, we choose the semi-implicit AOS scheme to improve the stability and accelerate the convergence. This scheme was first proposed in [34] and later applied to nonlinear diffusion filtering [35]. It is unconditionally stable and does not suffer from the time step restriction. The AOS scheme splits an arbitrary d-dimensional spatial operator into a set of one-dimensional ones and computes implicitly in parallel by the Thomas algorithm efficiently.

Specially for (46), we solve the following semi-implicit equation by the AOS scheme for $n=0,1,\ldots,N-1$:

$$\frac{\phi^{[k,n+1]}-\phi^{[k,n]}}{\Delta t}=\mu\Delta\phi^{[k,n+1]}+\nabla\cdot\left[(\lambda^k-\mu)\frac{\nabla\phi^{[k,n+1]}}{|\nabla\phi^{[k,n]}|}\right]+\alpha\delta_\varepsilon(\phi^{[k,n]})\nabla\cdot\left(\frac{\nabla\phi^{[k,n+1]}}{|\nabla\phi^{[k,n]}|}\right)+\delta_\varepsilon(\phi^{[k,n]})\big[\beta_1(I-c_1^k)^2-\beta_2(I-c_2^k)^2\big], \tag{48}$$

with $\phi^{[k,0]}=\phi^k$. The solution of (47) by the AOS scheme is similar to (48). For full discretization, we use finite differences [15] to discretize the spatial partial derivatives.

Though it is not very expensive in calculation of one semi-implicit step, the total computational effort of one outer iteration requiring many inner steps can be very huge. In order to reduce the computational effort while keeping effectiveness, we simplify the inner-outer iterative framework of each algorithm by performing only one step (i.e., $N=1$) in the inner iteration using the AOS scheme. The resulting alternating algorithms are very efficient from numerical experience.

The evolution can be stopped if some stopping criterion is satisfied. In our paper, we employ a criterion for CV model recently proposed in [36]. The iteration will be stopped automatically when the change of the curve length keeps smaller than a prescribed threshold θ_{length} for a fixed threshold of iterations $\mathcal{M}$.

Now we are ready to present the algorithms for the CV model.

Remark 2 The proposed two algorithms can be generalized to the multi-phase CV model [29] to eliminate the need of reinitialization.

Remark 3 For all our implementation of the Uzawa algorithm, we have set μ to be constant during the iterations. Better convergence behavior may be obtained if μ is increased gradually. But instability may be caused if μ is increased too quickly, which is a common phenomenon when using the augmented Lagrangian approach [24].

Remark 4 We have used variable splitting and the penalty approach for the projection Lagrangian algorithm. Then one drawback exists that as γ becomes very large, the intermediate minimization problems become increasingly ill-conditioned. Then numerical problems will be caused [24, 27]. Therefore, we should choose moderate values of γ in simulation.

5 Computational Results

In this section, some numerical results for qualitative and quantitative comparisons among different methods are presented to demonstrate the effectiveness and efficiency of our algorithms. We refer the Algorithm 3, Algorithm 4 and the penalty method of [14] applying to CV model respectively as UA, PLA and Li's method in the following. We set $\beta_1 = \beta_2 = 1$ for generality. The initial LSF ϕ^0 is a piecewise constant function with a rectangular contour located in the middle of the image to be segmented for our methods and Li's method. For the VLSM with reinitialization, the initial LSF is a signed distance function. The parameter α is usually formatted by $\alpha = \eta \times 255^2$, $\eta \in (0, 1)$. We set the spatial step $h = 1$ and the parameter $\varepsilon = 1.5$. For the stopping criterion, we use $\theta_{length} = 5$ and $\mathcal{M} = 10$ as in [36].

First, we use the natural Europe night-lights image to illustrate the unfavorable effects of reinitialization for the CV model in Fig. 1. We can see from Figs. 1(b) and 1(c) that the segmented images visually have different topologies for the VLSM with no or with reinitialization process using the same parameters, which demonstrates that whether or not the reinitialization is done affects segmentation results. For reinitialization, we have used the first order upwind scheme [30] to solve (6) with ten time marching steps and implement this procedure for every fifth iteration. Then the segmentation results by Li's method and our methods given in Fig. 2 show the effectiveness of the three algorithms. Moreover, they show that Li's method and the presented methodology incorporating the reinitialization constraint variationally do not suffer from the same unfavorable effects as the classical reinitialization. See Tables 1 and 2 for the corresponding iteration number and cost time for segmentation of this example. For the VLSM with reinitialization, more than half of the time is spent on reinitialization. Li's method has faster implementation although it requires more iterations than the VLSM with reinitialization. We can see that our methods are much faster than both of the VLSM and Li's method.

Algorithm 3 Uzawa Algorithm for VLSMWR applying to CV model

Choose μ properly, fixed. Initialization: ϕ^0, λ^0, $k = 0$.

Step 1. Update c_1, c_2 by (44) and (45).
Step 2. Update ϕ by solving (46) using the semi-implicit AOS scheme (48) with $N = 1$.
Step 3. Update λ by (25).
Step 4. Test whether the stopping criterion is satisfied. If yes, the algorithm is stopped. Otherwise, set $k = k + 1$ and continue.

Algorithm 4 Projection Lagrangian Algorithm for VLSMWR applying to CV model

Choose γ properly, fixed. Initialization: ϕ^0, $\mathbf{p}^0$, λ^0, $k = 0$.

Step 1. Update c_1, c_2 by (44) and (45).
Step 2. Update ϕ by solving (47) using the AOS scheme with $N = 1$.
Step 3. Update $\mathbf{p}$ by (39).
Step 4. Update λ by (41).
Step 5. Test whether the stopping criterion is satisfied. If yes, the algorithm is stopped. Otherwise, set $k = k + 1$ and continue.

Then we compare our methods with Li's method by a spiral image from an art picture. The original image shown in Fig. 3(a) is processed by Li's method and our methods, respectively. As shown in Fig. 4, our two methods can also detect features as Li's method for the same image. We observe from Table 2 that either of our algorithms exceeds Li's method in the convergence speed and computational time.

We show further the robustness and accuracy of our methods by a synthetic binary image. The original binary image with ground truth known a priori is presented in Fig. 5(a). Then the image is imposed with the Gaussian additive noise in Fig. 5(b). The Signal to Noise Ratio (SNR), which is defined as

$$\mathrm{SNR} = 10 \cdot \log_{10}\left(\frac{\text{Variance of Data}}{\text{Variance of Noise}}\right),$$

for this image is 4.41.

The degraded image is segmented by the VLSM with reinitialization, Li's method and the two proposed methods,

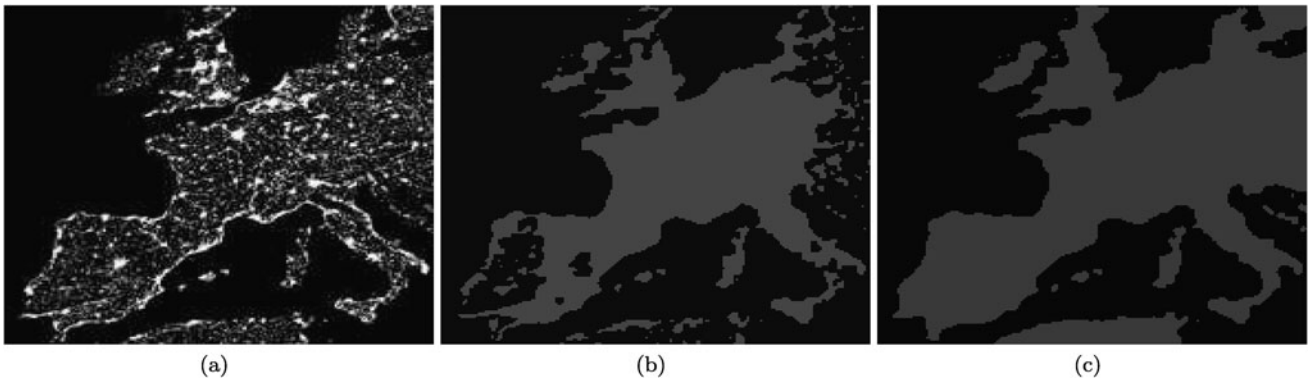

Fig. 1 Segmentation of Europe night-lights image using VLSM with no reinitialization and with reinitialization for $\alpha = 0.08 \times 255^2$ and $\Delta t = 0.01$. (**a**) Original Europe night-lights image. (**b**) Processed image with no reinitialization. (**c**) Processed image with reinitialization for every fifth iteration

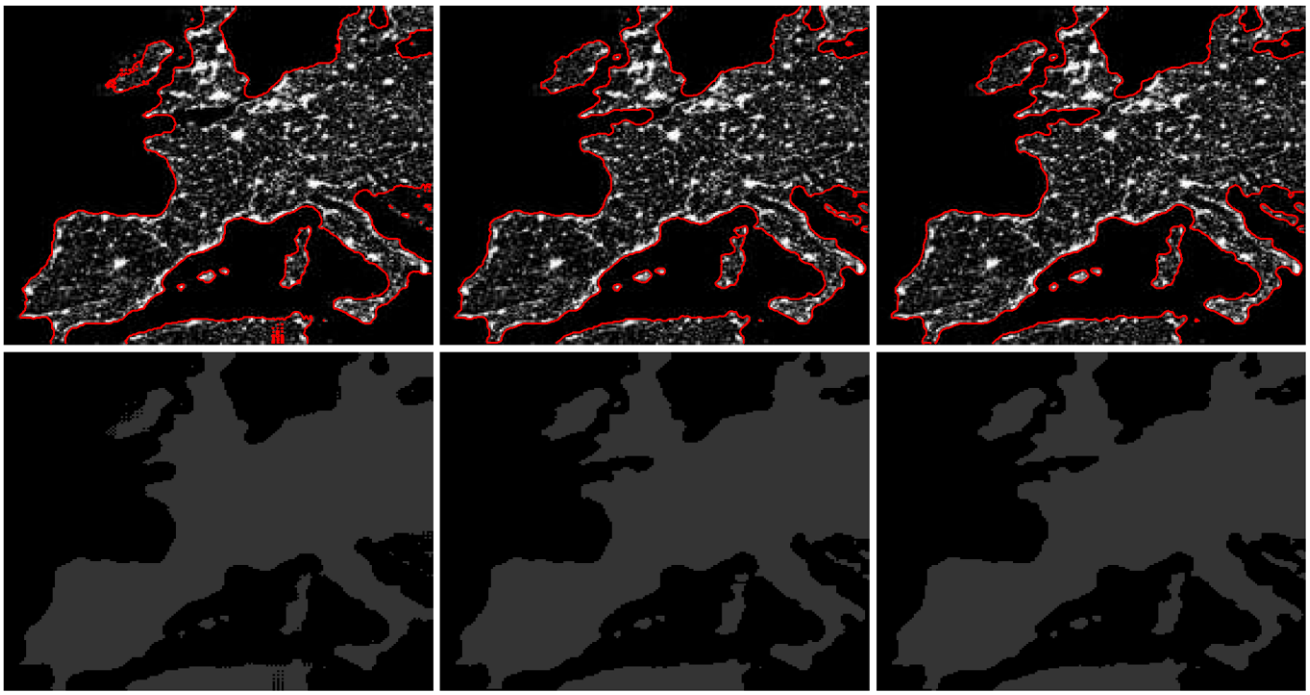

Fig. 2 Segmentation of Europe night-lights image using Li's method, UA and PLA, respectively. *First column*: Segmentation result using Li's method with $\alpha = 0.15 \times 255^2$, $\mu = 1$, $\Delta t = 0.02$ and the piecewise constant approximation. *Second column*: Segmentation result using UA with $\alpha = 0.05 \times 255^2$, $\mu = 0.01$, $\Delta t = 0.05$ and the piecewise constant approximation. *Third column*: Segmentation result using PLA with $\alpha = 0.06 \times 255^2$, $\gamma = 0.1$, $\Delta t = 0.1$ and the piecewise constant approximation

Table 1 Comparisons on the computational effort between our methods and the VLSM with reinitialization

Images (size)	VLSM with reinitialization			UA		PLA	
	Iterations	Time (s)	R-Time[a] (s)	Iterations	Time (s)	Iterations	Time (s)
Europe night-lights (180 × 195)	247	16.42	9.8	45	2.48	67	4.19
Synthetic image (128 × 128)	30	4.26	3.51	18	0.47	13	0.37

[a]The time spent on reinitialization

Table 2 Comparisons on the computational effort between our methods and Li's method

Images (size)	Li's method		UA		PLA	
	Iterations	Time (s)	Iterations	Time (s)	Iterations	Time (s)
Europe night-lights (180 × 195)	331	13.83	45	2.48	67	4.19
Spiral (187 × 227)	285	15.48	61	4.56	69	5.11
Synthetic image (128 × 128)	76	1.42	18	0.47	13	0.37
Ultrasound (202 × 241)	184	11.02	24	1.96	18	1.53
Galaxy (140 × 179)	183	5.74	26	1.05	51	2.45

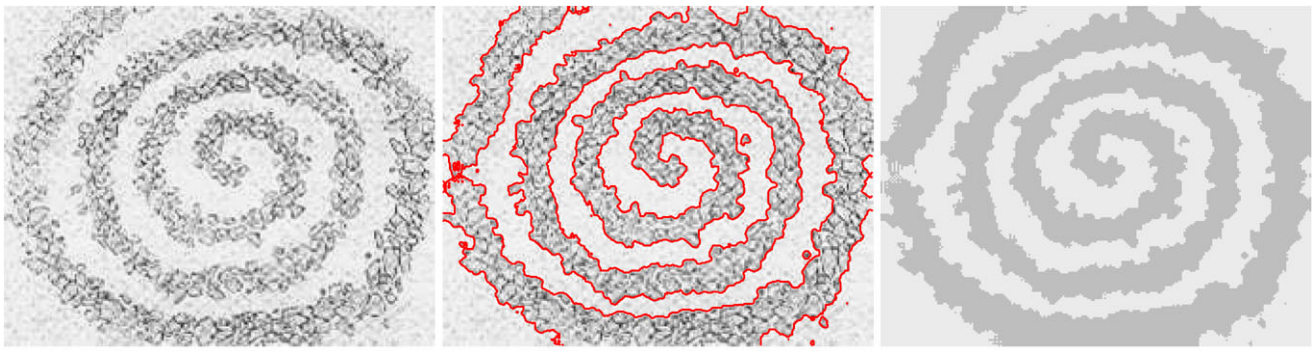

Fig. 3 Segmentation of the spiral image using Li's method. (**a**) The original spiral image. (**b**) Segmentation result using Li's method with $\alpha = 0.05 \times 255^2$, $\mu = 1$, $\Delta t = 0.02$. (**c**) The piecewise constant approximation

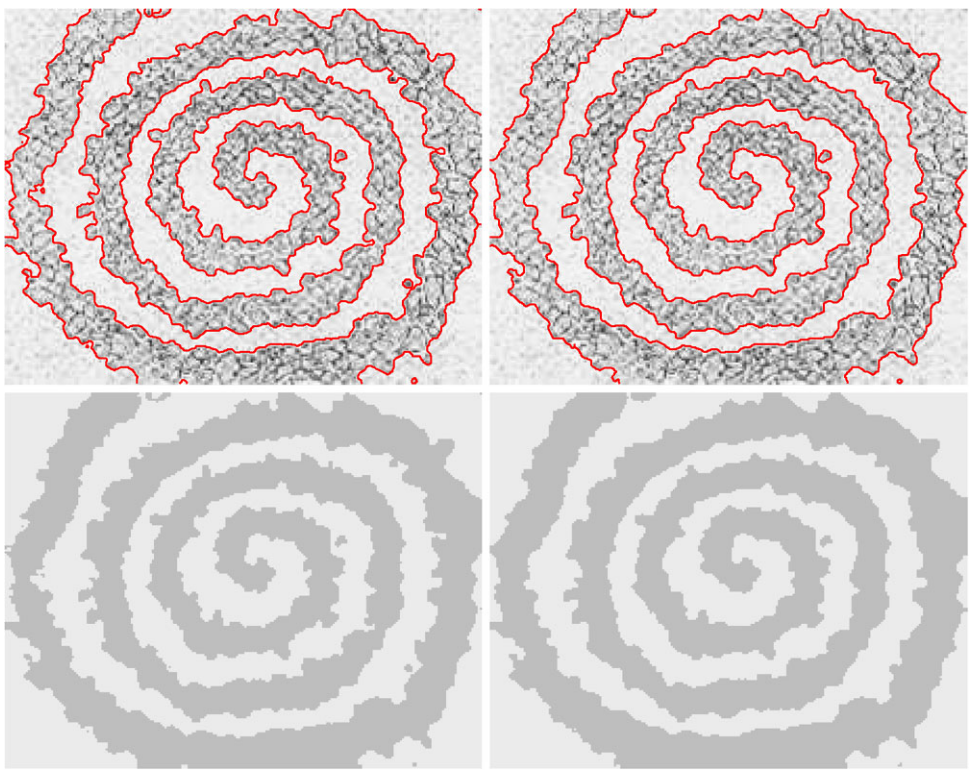

Fig. 4 Segmentation of the spiral image using UA and PLA, respectively. *First column*: Segmentation result using UA with $\alpha = 0.04 \times 255^2$, $\mu = 0.001$, $\Delta t = 0.1$ and the piecewise constant approximation. *Second column*: Segmentation result using PLA with $\alpha = 0.05 \times 255^2$, $\gamma = 1$, $\Delta t = 0.03$ and the piecewise constant approximation

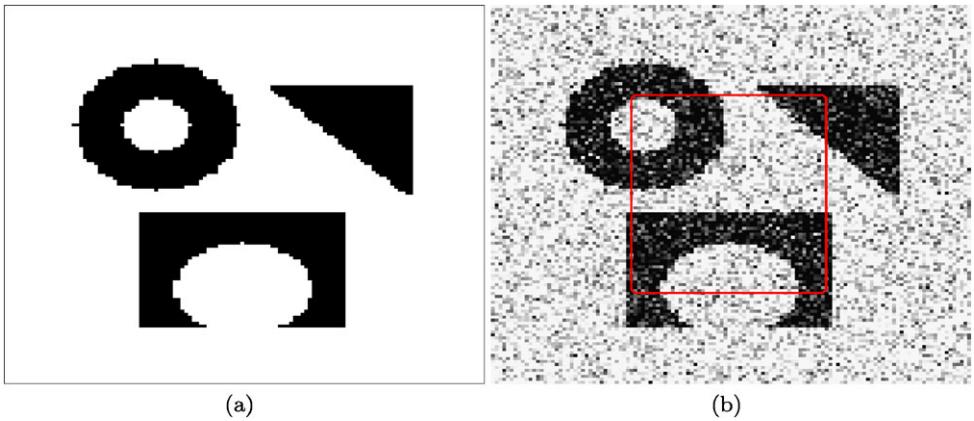

Fig. 5 (**a**) Original synthetic image. (**b**) Degraded image and the same initial contour for all the methods

respectively. We use the same initial contour as shown in Fig. 5(b) for all these approaches. The intermediate iterations and the final results are displayed in Fig. 6. From the satisfactory results, we can see that all the four methods work for this noisy image. In Fig. 7, we present quantitative comparisons among the four methods by giving the plots of the L^2-Error (i.e., L^2 distance between the characteristic function of the segmented object and that of the exact object) vs. the iteration number and the time spent, respectively. We observe from Fig. 7 that our methods converge faster and give more accurate segmentation results. Then we investigate the influence of the parameter μ in Table 3 by increasing μ gradually while fixing other parameters as $\alpha = 0.15 \times 255^2$ and $\Delta t = 0.02$. We can see from Table 3 that a small value of μ leads to quantitatively better segmentation. But it also shows that the segmentation error and iteration number keep unchanged as $\mu \leq 10^{-2}$. Therefore, we need not use very large or small μ in the augmented Lagrangian method. Meanwhile, the time reported in Tables 1 and 2 shows a large reduction in the total computation effort by our algorithms.

In Fig. 8, we show the segmentation of an ultrasound medical image by Li's method and our methods, respectively. All the three algorithms can detect the cell in the image. Again, the time reported in Table 2 shows more efficiency of our methods. Moreover, we use this example to investigate the role of the penalty parameters μ and γ for our methods. In Fig. 9, we plot the mean deviation of $|\nabla\phi^k| - 1$, which measures the distance between the computed LSF at the kth iteration and the signed distance function of the same zero contour. We observe that the constraint $|\nabla\phi| = 1$ can be satisfied better as μ or γ increases. Considering the segmentation accuracy, however, the time step should be decreased accordingly.

In Fig. 10, we present segmentation results of a galaxy image with scattered data shown in Fig. 10(a) using Li's method to illustrate the influence of the penalization parameter μ. Since the segmentation results are largely dependent on the weighted parameters of the regularization term and the data fitting terms, especially for images with very smooth contours [15], we use the same fixed value $\alpha = 0.01 \times 255^2$ and investigate the role of the parameter μ. We observe that when μ increases from 0.01 to 10, the segmentation result becomes more visually pleasing, which coincides well with the property of the penalty method. That is, we should use relatively large penalty parameter in Li's method especially for the segmentation of challenging images such as this galaxy image. However, the time step (from 1 to 0.02) must be small enough to ensure stability of the algorithm, which slows down the convergence of the algorithm. In Table 2, we report the computational effort for Fig. 10(d).

Table 3 Effect of μ on the converged value of L^2-Error

μ	Converged L^2-Error	Iterations
10^{-3}	5.3852	19
10^{-2}	5.3852	19
10^{-1}	5.7446	19
1	5.8310	22

Figure 11 displays segmentation of the galaxy image using UA. We use the same value for α as in Fig. 10 for comparability. When μ changes from 10^{-4} to 1, the segmentation results are visually similar to that obtained by Li's method with larger $\mu = 10$. Therefore, we conclude that it is enough to choose a relatively small μ in the augmented Lagrangian method as mentioned previously. Figure 12 shows the results using PLA. The iteration numbers for the two different parameters $\gamma = 1$ and $\gamma = 10$ are 58 and 51, respectively. Therefore, the total time is almost the same. Once again, from Table 2, we can see the superiority of our two algorithms to Li's method in efficiency.

Since the AOS scheme we have employed needs the solution of linear systems, the computational effort for each iteration of our algorithms is higher than that of Li's method. However, we can see from Table 2 that the total compu-

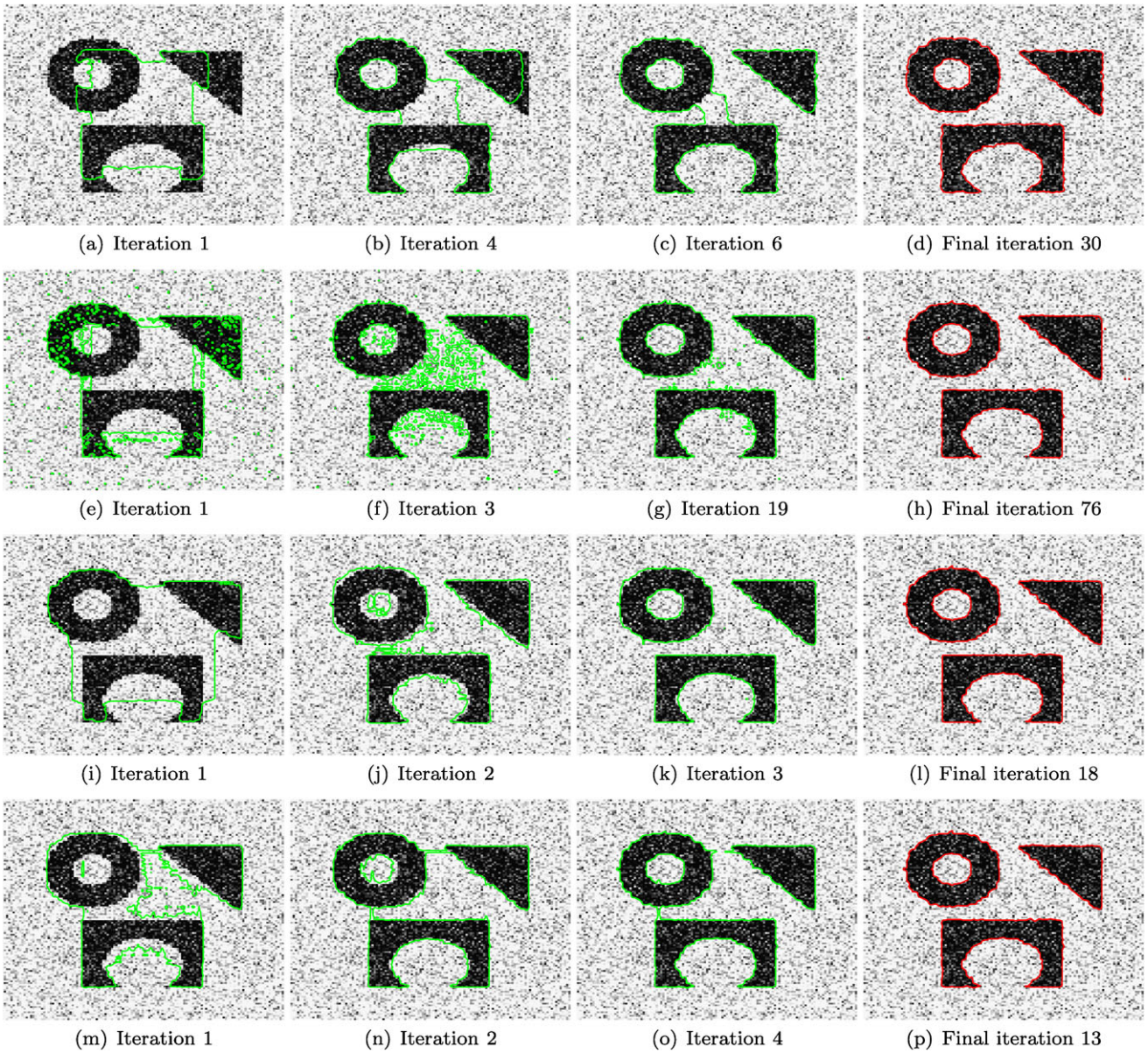

Fig. 6 Segmentation of the noisy synthetic image using VLSM with reinitialization, Li's method, UA and PLA, respectively. *First row*: Evolution using VLSM with reinitialization with $\alpha = 0.3 \times 255^2$, $\Delta t = 0.01$. *Second row*: Evolution using Li's method with $\alpha = 0.35 \times 255^2$, $\mu = 1$, $\Delta t = 0.02$. *Third row*: Evolution using UA with $\alpha = 0.15 \times 255^2$, $\mu = 1$, $\Delta t = 0.02$. *Fourth row*: Evolution using PLA with $\alpha = 0.15 \times 255^2$, $\gamma = 1$, $\Delta t = 0.1$

tational cost required by our approaches is much less than Li's method due to the significant reduction in the iteration number.

Choosing the time step needs a practical consideration [35]. An unpractically large time step will influence the accuracy of the segmentation and cause oscillations. Therefore, we do not choose very large time steps in our experiments even if the AOS scheme does not suffer from any time step restriction.

Both of the proposed iterative algorithms are based on gradient descent type evolution of the LSF. The PLA requires to solve one more subproblem (w.r.t. $\mathbf{p}$) than UA at each iteration. By virtue of the extremely fast weighted shrinkage operator, however, the additional computational effort for solving this subproblem is nearly negligible comparing with the solution of linear equations required by the AOS scheme. From the above experiments, we basically conclude that both of the two methods are very effective and efficient. It is difficult to say which one is better in effectiveness, efficiency and accuracy.

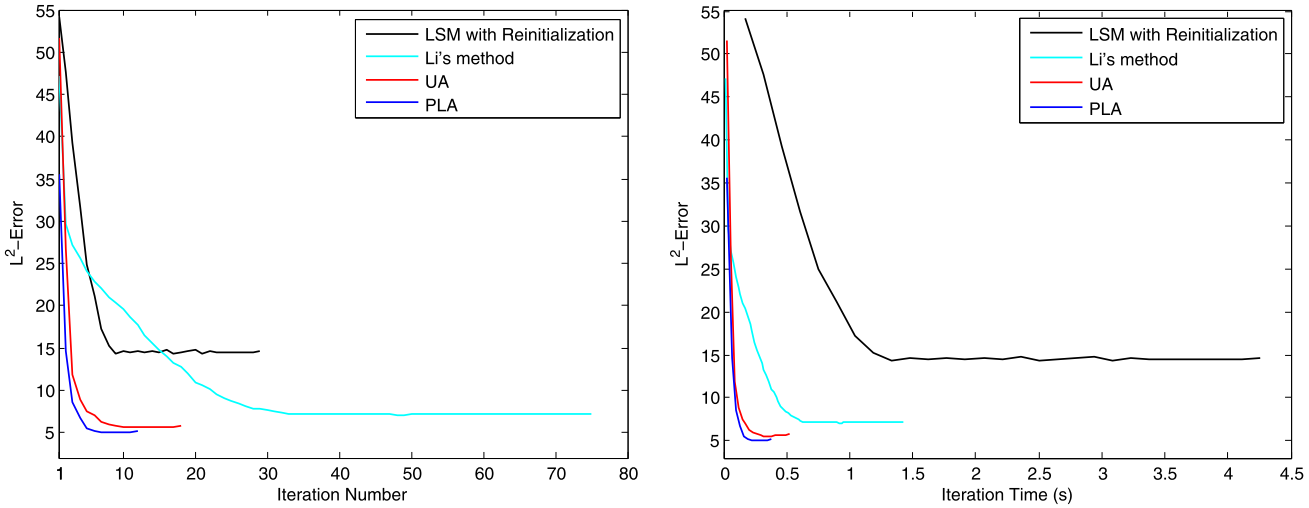

Fig. 7 Evolution of L^2-Error for segmentation of the synthetic image using different methods. *Left*: L^2-Error vs. iteration number. *Right*: L^2-Error vs. iteration time

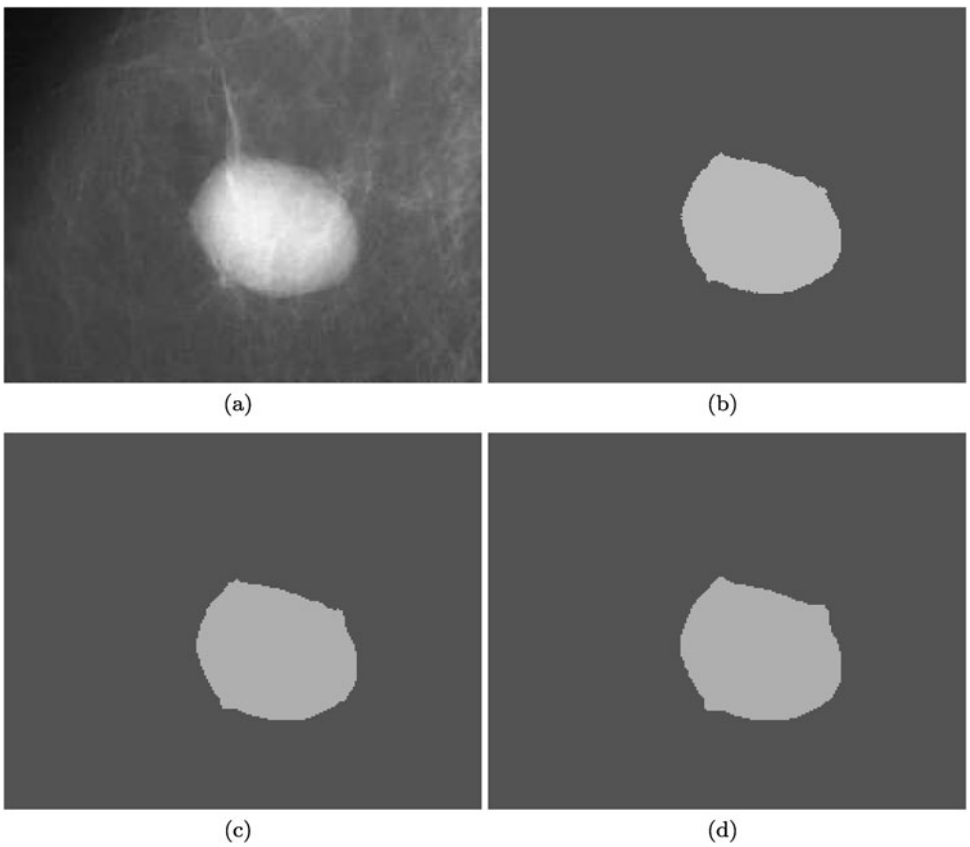

Fig. 8 Segmentation of the ultrasound image using three different methods. (**a**) Original ultrasound image. (**b**) Processed image using Li's method with $\alpha = 0.05 \times 255^2$, $\mu = 1$, $\Delta t = 0.1$. (**c**) Processed image using UA with $\alpha = 0.05 \times 255^2$, $\mu = 0.01$, $\Delta t = 0.2$. (**d**) Processed image using PLA with $\alpha = 0.1 \times 255^2$, $\gamma = 1$, $\Delta t = 0.02$

6 Conclusions and Future Work

We have eliminated the requirement of reinitialization in the VLSM by the augmented Lagrangian method and the projection Lagrangian method for constrained optimization. For the augmented Lagrangian method, we employed the effective Uzawa type algorithm. Numerical results showed that we could get stable segmentation by choosing a small penalization parameter in a large range. For the updating scheme of the projection Lagrangian method, we introduced an auxiliary variable to deal with the gradient term. In this way, we obtained a simple and explicit updating formulation of

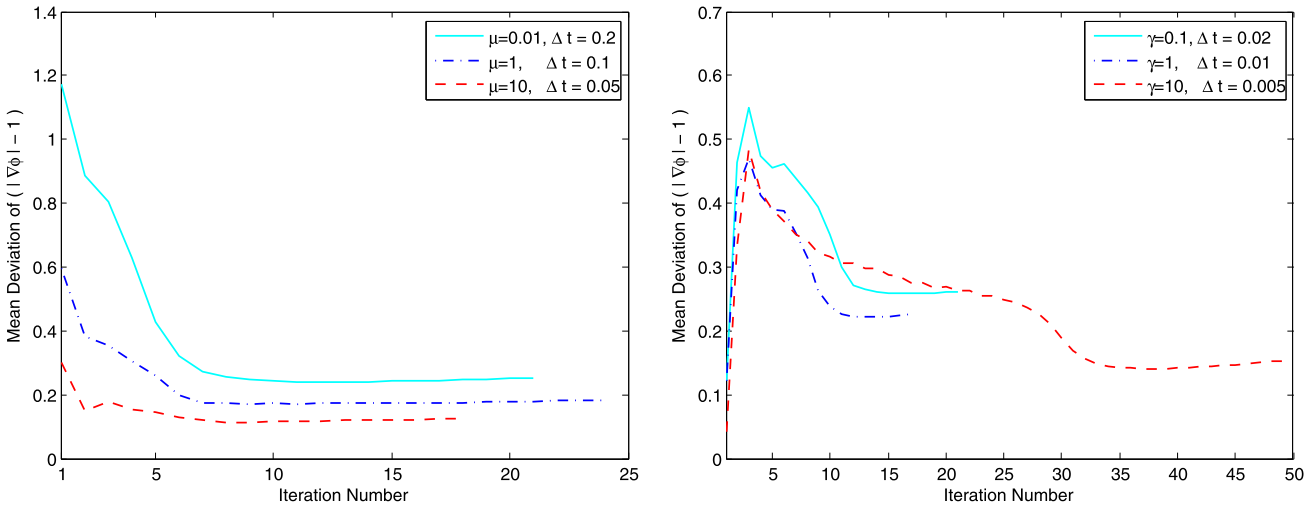

Fig. 9 Evolution of mean deviation of $(|\nabla\phi| - 1)$ for the ultrasound image using UA (*left*) and PLA (*right*)

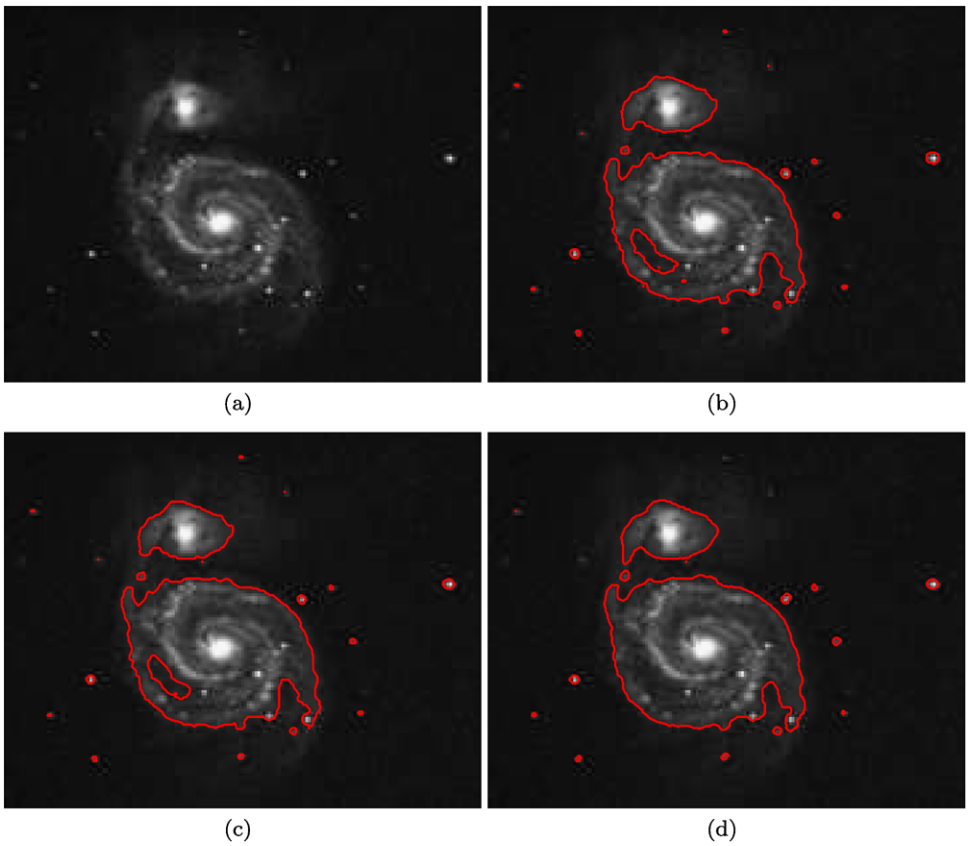

Fig. 10 Segmentation of the galaxy image using Li's method with $\alpha = 0.01 \times 255^2$ but different values of μ. (**a**) Original image. (**b**) Processed image with $\mu = 0.01$, $\Delta t = 1$. (**c**) Processed image with $\mu = 0.1$, $\Delta t = 0.5$. (**d**) Processed image with $\mu = 10$, $\Delta t = 0.02$

the Lagrange multiplier. The traditional LSM implements the reinitialization apart from the evolution by solving additional PDEs, while our methods incorporate the reinitialization process into the same evolution equation. Therefore, our approaches do not have the problems such as whether to implement the reinitialization process, when and how to implement the reinitialization.

Then we applied the proposed methods to the CV model and presented two efficient algorithms by virtue of the semi-implicit AOS scheme, which improved the stability and reduced the total computational effort of our algorithms. Numerical experiments have demonstrated that our algorithms have no unfavorable effects on segmentation results as traditional reinitialization techniques. Moreover, various numer-

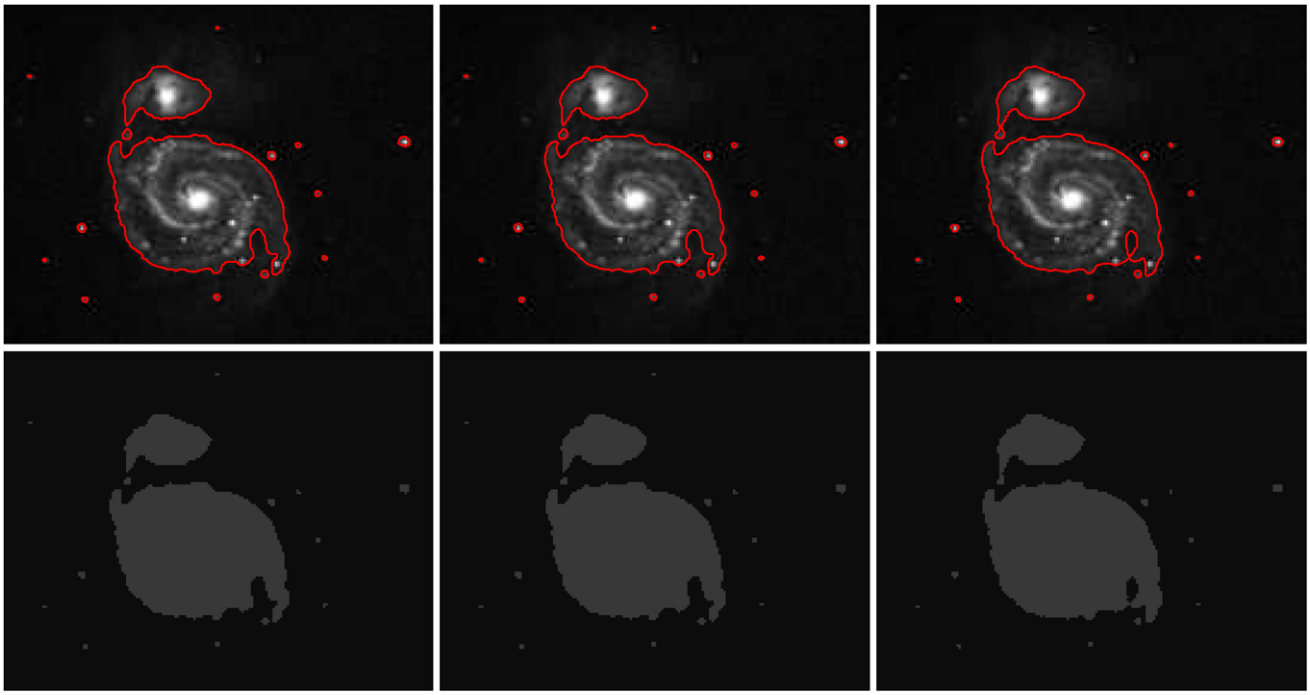

Fig. 11 Segmentation of the galaxy image using UA with $\alpha = 0.01 \times 255^2$ but different values of μ. *First column*: Segmentation results with $\mu = 10^{-4}$, $\Delta t = 0.2$. *Second column*: Segmentation results with $\mu = 10^{-3}$, $\Delta t = 0.2$. *Third column*: Segmentation results with $\mu = 10^{-1}$, $\Delta t = 0.1$

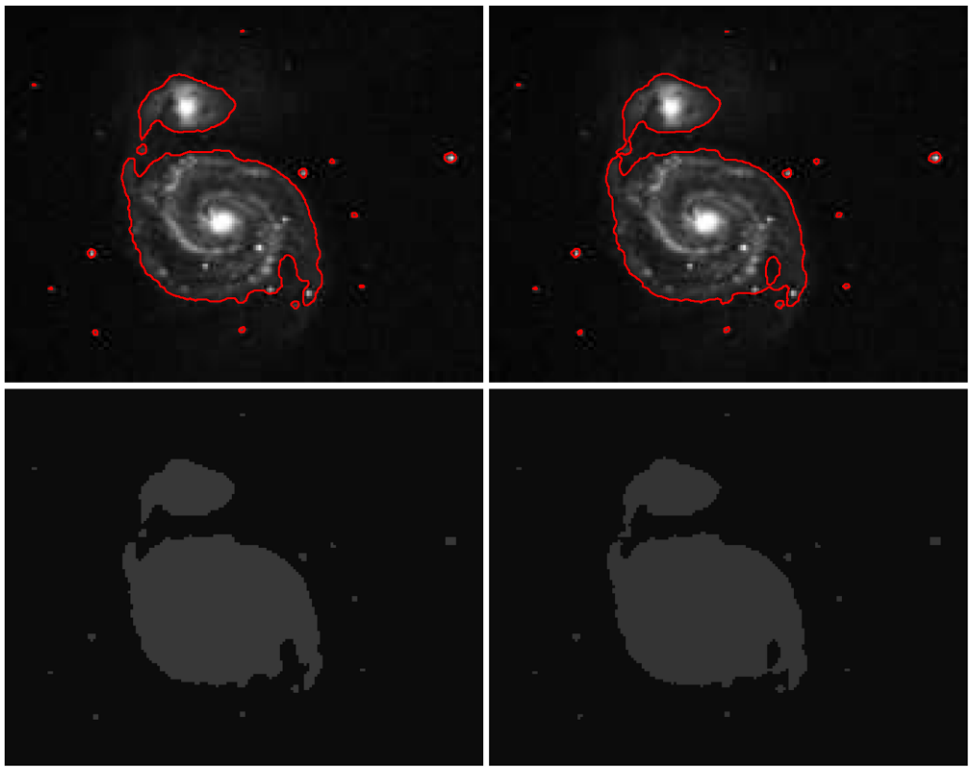

Fig. 12 Galaxy image processed using PLA with $\alpha = 0.01 \times 255^2$ but different values of γ. *First column*: Segmentation results with $\gamma = 1$, $\Delta t = 0.1$. *Second column*: Segmentation results with $\gamma = 10$, $\Delta t = 0.05$

ical comparisons show that our algorithms are robust and more efficient than other approaches.

The proposed methods can generally be extended to the multiphase case with multiple LSFs. Our future work includes applications of our methods to other two phase and multiphase problems using LSM with the reinitialization process, for example, topology optimization, shape reconstruction and other imaging and vision tasks.

Acknowledgements The authors express their sincere thanks to the reviewers for constructive suggestions and valuable comments, which greatly improved the original manuscript. This work was supported in part by the NNSF of China (Grant No. 10971190) and the Qiu-Shi Chair Professor Fellowship from Zhejiang University.

References

1. Osher, S., Sethian, J.A.: Fronts propagation with curvature dependent speed: algorithms based on Hamilton-Jacobi formulations. J. Comput. Phys. **79**, 12–49 (1988)
2. Sethian, J.A., Wiegmann, A.: Structural boundary design via level set and immersed interface methods. J. Comput. Phys. **163**, 489–528 (2000)
3. Osher, S., Santosa, F.: Level set methods for optimization problems involving geometry and constraints I. frequencies of a two-density inhomogeneous drum. J. Comput. Phys. **171**, 272–288 (2001)
4. Sussman, M., Smereka, P., Osher, S.: A level set approach for computing solutions to incompressible two phase flow. J. Comput. Phys. **114**, 146–159 (1994)
5. Santosa, F.: A level-set approach for inverse problems involving obstacles. ESAIM Control Optim. Calc. Var. **1**, 17–33 (1996)
6. Chan, T.F., Tai, X.-C.: Level set and total variation regularization for elliptic inverse problems with discontinuous coefficients. J. Comput. Phys. **193**, 40–66 (2003)
7. Fedkiw, R.P., Sapiro, G., Shu, C.-W.: Shock capturing, level sets, and PDE based methods in computer vision and image processing: a review of Osher's contributions. J. Comput. Phys. **185**, 309–341 (2003)
8. Osher, S., Paragios, N.: Geometric Level Set Methods in Imaging, Vision and Graphics. Springer, Berlin (2003)
9. Sethian, J.A.: Level Set Methods and Fast Marching Methods. Cambridge University Press, Cambridge (1999)
10. Osher, S., Fedkiw, R.: Level Set Methods and Dynamic Implicit Surfaces. Springer, Berlin (2003)
11. Tai, X.-C., Chan, T.F.: A survey on multiple level set methods with applications for identifying piecewise constant functions. Int. J. Numer. Anal. Mod. **1**, 25–48 (2004)
12. Gomes, J., Faugeras, O.: Reconciling distance functions and level sets. J. Vis. Commun. Image Represent. **11**, 209–223 (2000)
13. Lie, J., Lysaker, M., Tai, X.-C.: A binary level set model and some applications to Mumford-Shah image segmentation. IEEE Trans. Image Process. **15**, 1171–1181 (2006)
14. Li, C., Xu, C., Gui, C., Fox, M.D.: Level set evolution without reinitialization: a new variational formulation. In: IEEE Computer Society Conference on Computer Vision and Pattern Recognition (CVPR), vol. 1, pp. 430–436 (2005)
15. Chan, T.F., Vese, L.A.: Active contours without edges. IEEE Trans. Image Process. **10**, 266–277 (2001)
16. Sethian, J.A.: A fast marching level set method for monotonically advancing fronts. Proc. Natl. Acad. Sci. **93**, 1591–1595 (1996)
17. Sethian, J.A.: Fast marching methods. SIAM Rev. **41**, 199–235 (1999)
18. Tsai, Y.-H.R., Cheng, L.-T., Osher, S., Zhao, H.-K.: Fast sweeping algorithms for a class of Hamilton-Jacobi equations. SIAM J. Numer. Anal. **41**, 673–694 (2003)
19. Adalsteinsson, D., Sethian, J.A.: The fast construction of extension velocities in level set methods. J. Comput. Phys. **148**, 2–22 (1999)
20. Peng, D., Merriman, B., Osher, S., Zhao, H., Kang, M.: A PDE-based fast local level set method. J. Comput. Phys. **155**, 410–438 (1999)
21. Lie, J., Lysaker, M., Tai, X.-C.: A variant of the level set method and applications to image segmentation. Math. Comput. **75**, 1155–1174 (2006)
22. Zhu, S., Wu, Q., Liu, C.: Variational piecewise constant level set methods for shape optimization of a two-density drum. J. Comput. Phys. **229**, 5062–5089 (2010)
23. Zhu, S., Liu, C., Wu, Q.: Binary level set methods for topology and shape optimization of a two-density inhomogeneous drum. Comput. Methods Appl. Mech. Eng. **199**, 2970–2986 (2010)
24. Nocedal, J., Wright, S.J.: Numerical Optimization. Springer, New York (1999)
25. Goldstein, T., Osher, S.: The split Bregman method for L1-regularized problems. SIAM J. Imaging Sci. **2**, 323–343 (2009)
26. Huang, Y., Ng, M., Wen, Y.: A new total variation method for multiplicative noise removal. SIAM J. Imaging Sci. **2**, 20–40 (2009)
27. Bioucas-Dias, J.M., Figueiredo, M.A.T.: Multiplicative noise removal using variable aplitting and constrained optimization. IEEE Trans. Image Process. **19**, 1720–1730 (2010)
28. Chan, T.F., Sandberg, B.Y., Vese, L.A.: Active contours without edges for vector-valued images. J. Vis. Commun. Image Represent. **11**, 130–141 (2000)
29. Vese, L.A., Chan, T.F.: A multiphase level set framework for image segmentation using the Mumford and Shah model. Int. J. Comput. Vis. **50**, 271–293 (2002)
30. Sussman, M., Fatemi, E.: An efficient, interface preserving level set redistancing algorithm and its application to interfacial incompressible fluid flow. SIAM J. Sci. Comput. **20**, 1165–1191 (1999)
31. Zhao, H.K., Chan, T.F., Merriman, B., Osher, S.: A variational level set approach to multiphase motion. J. Comput. Phys. **127**, 179–195 (1996)
32. Tai, X.-C., Wu, C.: Augmented Lagrangian method, dual methods and split Bregman iteration for ROF model. UCLA CAM Report 09-05 (2009)
33. Mumford, D., Shah, J.: Optimal approximations by piecewise smooth functions and associated variational problems. Commun. Pure Appl. Math. **42**, 577–685 (1989)
34. Lu, T., Neittaanmäki, P., Tai, X.-C.: A parallel splitting up method and its application to Navier-Stokes equations. Appl. Math. Lett. **4**, 25–29 (1991)
35. Weickert, J., Romeny, B.M., Viergever, M.A.: Efficient and reliable schemes for nonlinear diffusion filtering. IEEE Trans. Image Process. **7**, 398–410 (1998)
36. Wang, X., Huang, D., Xu, H.: An efficient local Chan-Vese model for image segmentation. Pattern Recognit. **43**, 603–618 (2010)

Chunxiao Liu received her B.S. degree from Linyi University in 2006. She is currently pursuing the Ph.D. degree in Center of Mathematical Sciences from Zhejiang University. The subject of her Ph.D. dissertation is image segmentation and restoration. Her main research interests are image processing and inverse problems.

Fangfang Dong received the Ph.D. degree in the Center of Mathematical Sciences from Zhejiang University, China, in 2010. Currently, she is a lecturer in the School of Statistics and Mathematics, Zhejiang Gongshang University. Her research interests include mathematical methods in image processing such as partial differential equation, variational methods and optimization theory.

Shengfeng Zhu received his B.S. degree from Zhejiang University in 2006. He is currently pursuing the Ph.D. degree in the Department of Mathematics at Zhejiang University, and his main topic is the study of numerical methods for shape optimization and geometric inverse problems. His research interests include numerical solutions of differential equations, optimal shape design and inverse problems.

Dexing Kong received his Ph.D. degree in the Institute of Mathematics from Fudan University in 1993, and then worked at Harvard University as post-doctoral research fellow, City University of Hong Kong as adjunct professor, and the International Centre for Theoretical Physics in Italy as visiting scientist. He is currently a Qiu-Shi Chair Professor in the Department of Mathematics at Zhejiang University. His research interests include partial differential equations, mathematical physics, geometric analysis and medical image processing.

Kefeng Liu received his Ph.D. degree from Harvard University in 1993 and then worked in Department of Mathematics at MIT as a Moore Instructor, Stanford University as an assistant professor, and UCLA as an associate professor. From 2002 to present, he has been a professor of Department of Mathematics at UCLA. He is currently a Guangbiao Chair Professor of Center of Mathematical Sciences and Department of Mathematics at Zhejiang University. His research interests include differential geometry, topology, mathematical physics and applied mathematics.